Synthesis of Zirconium based metal organic frameworks (Zr-UiO-66) for enhanced adsorptive removal of water contaminants

Sultan Ahmed, Salim Samra, W. S. Abo El-Yazeed and Awad I. Ahmed

Chemistry Department, Faculty of science, Mansoura University, Mansoura, Egypt

* Correspondence to: *awahmed@mans.edu.eg 01001645969*

Abstract: Methylene blue dye is among the most popular dyes that have bad effects on aquatic life, so many efforts were directed to remove it from the environment. Our study aims to prepare a zirconium metal-organic framework called UiO-66 MOF to use it in the MB adsorption. (FTIR) and (SEM) were used how to describe the structural and microstructural the UiO-66 MOF. The prepared MOF revealed a significant adsorption capacity for MB reaching 70.29 mg/g. Researchers studied investigated how such parameters, including concentration, pH, temperature, weight and contact time altered the adsorption process. Meanwhile, the adsorption isotherms and kinetics were studied. The pseudo 2nd order kinetic and Langmuir adsorption isotherm models were found to be the most accurate descriptions of MB adsorption on the UiO-66 MOF.

1.Introduction

Recently, (MOFs) have gained great attention as a series of porous substances [1]. MOFs are crystalline, sponge-like, porous nanomaterials consisting of metal ions connected to ligands to form structures that can be porous with repeating building blocks represented in 1, 2, or 3 dimensions [2]. Many researchers are concerned with studying different preparation methods and applications of many MOF versions. The properties of the MOFs as post-synthesis treatment, tunable pore size, high surface area, and incorporation of various functionalities give them unexpected importance [3-5] in wastewater treatment processes, sensing, drug delivery, metal extraction, biomedical, supercapacitors, energy storage, gas adsorption and separation and catalysis [6-11]. The diversity of transition metals and the variety in the structure of the ligands also give MOF materials significant importance. Zirconium MOF (Zr-MOF) is one of more than 20000 known MOFs with a high degree of stability in liquid phase reactions [12]. UiO-66 and UiO-67 are two types of zirconium-based MOFs that differ in the type of organic linker which is For UiO-66, 1,4-benzene dicarboxylic acid and biphenyl-4,4′-dicarboxylic acid in case of UiO-67 [13].

Besides that water and popular organic solvents, the two materials are extremely stable under high pressure and high temperatures. It was observed by UiO-66 was extremely effective in a variety of organic reactions, such as the cyclization of citronellal, the CO_2 cycloaddition of styrene oxide and cyclooctene epoxidation [14-16].

With the rapid development in industry, the amount of freshwater has decreased sharply while wastewater is increasing continuously. Many industries produce wastes such as herbicides, pharmaceuticals, personal care products, heavy metals, and dyes. Every year, approximately 9 million tons of dyes are manufactured [17] for use in the textile, food, and coloring sectors. But these dyes are carcinogenic and have many harmful effects on aquatic life, so they must be removed [18]. Many methods can be used for these purposes as adsorption, photocatalytic degradation, and catalytic oxidation [19,20]. One of the more frequent dyes to be removed from wastewater is MB, but there are obstacles to overcome, including material regeneration, a narrow pH range, and adsorbents with low adsorption capacities [21].Different adsorbents have been utilized to remove MB from wastewater as

metal oxides, zeolites, mesoporous carbons, graphene oxide, graphene, activated carbons, and MOFs [22-25]. Many MOFs were reported to use for adsorption of several dyes from aqueous systems such as Fe(BTC), magnetic $CU_3(BTC)_2$, MIL-125(Ti), and MOF(Co/Ni) [26-29].

2. Materials and methods

2.1. Materials

Zirconium Nitrate ($Zr(NO_3)_4$), dimethyl-formamide (DMF, $(CH_3)_2NCHO \geq 99.5\%$), Terephthalic (H_2BDC, $C_6 H_4 (COOH)_2$, 98%), methylene blue (MB) and Chloroform ($CHCL_3$) were used as obtained from commercial sources and used in the preparation of MOFs without further purification.

2.2. Zr-MOF (UiO-66) preparation:

Using a solvothermal technique, we manufactured UiO-66 in conformity with the prior literature [30]. 1 mmol of $Zr(NO_3)_4$ dissolved in 30 ml DMF was mixed well with 1 mmol H_2BDC and The mix was put into an autoclave and baked throughout 24 hours at 120 °C. Then, after first being reduced to room temperature, filtered, cleaned with DMF many times, and filtered again to obtain a white solid precipitate. The precipitate was dipped in 10 mL chloroform and replaced 3 times a day, then dry in an oven at 80 °C., yielding white powder crystals.

2.3. Characterization

A pristine Zr-MOF (UiO-66) was described using different techniques including (SEM, JEOL JSM 6510lv) and IR (FTIR, Thermo SCIENTIFIC NICOLET iS10).

2.4. Adsorption Experiment

Initially, we prepared a watery stock solution of MB (1000 ppm) by disappearing MB in distilled water. Then, different amounts of activated UiO-66 MOF materials were added to 50 ml of MB with an initial concentration from 25 to 250 mg/L. 0.1 M NaOH0.1 and M HCl were used to change the suspensions' pH. The adsorption equilibrium of MB was found to achieve after 12 h of stirring at room temperature and 250 rpm. The suspensions were filtered and then MB equilibrium concentrations were determined by spectrophotometer at λ_{max} value of 665 nm using the equation:

$$q_e = \frac{(C_o - C_e)v}{w}$$

Where Ce is the final concentrations of MB (mg/L), C_0 is the initial concentrations of MB (mg/L), V is the solution volume (mL) and W is the mass of UiO-66 MOF. Kinetic analyses were carried out to assess the MB absorption on adsorbents over time.

3. Results and Discussion

3.1. FTIR

UiO-66 MOF with a cubic lose-packed (CCP) structure was initially reported at the University of Oslo, resulting in nanosized pore materials [31]. By investigating the spectrum of UiO-66 MOF in Fig. 1, we can see the bands characteristic of the Zr-O bonds at 475, 659, and 752 cm^{-1} [31]. While the band at 1387 cm-1 corresponds to the C=C in aromatic ring, the bands that arise in the area 1500-1661 cm-1 are typical of C=O [32]. The bands at 2844 and 2924 represent the CH of the solvent (DMF). The absence of any beak around 1700 indicates that all carboxyl groups of terephthalic acid are deprotonated.
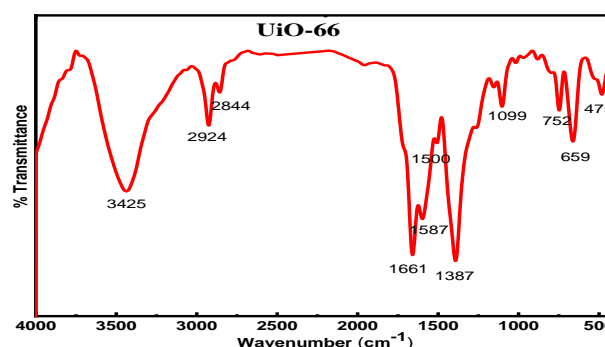
Fig 1: FTIR spectrum of UiO-66.

3.2. SEM

SEM was applied to explore morphology of the surface of synthetic UiO-66 and the image is shown in Fig 2. The image reveals particles of different sizes and irregular cubic shapes.
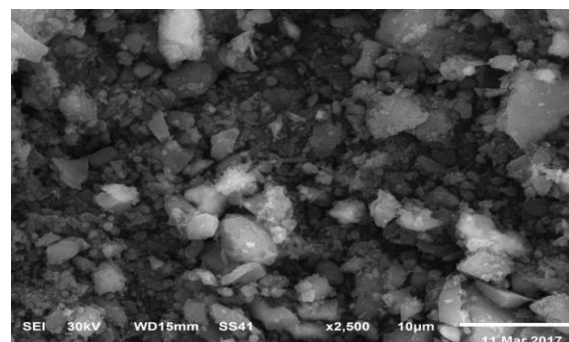
Fig 2: SEM image of UiO-66.

3.3. Adsorption of MB

3.3.1. Effect of pH

Different pH values were selected in the range of 4-12 at 25 °C and the initial concentration of MB was kept constant at 100 ppm. As shown in Fig 3, UiO-66 MOF revealed statistically significant MB removal in all pH values ranging from 4 to 12. By increasing the pH, the adsorption of MB increases till reaches the maximum at pH=10. So, pH=10 is selected for further experiments. At pH=4, the adsorption of MB, which is a cationic dye, is less due to the high concentration of H^+ at low pH which makes the surface charge of UiO-66 MOF positive. The significant negative charge on the surface of the UiO-66 MOF causes the adsorption of MB to increase at high pH [33].
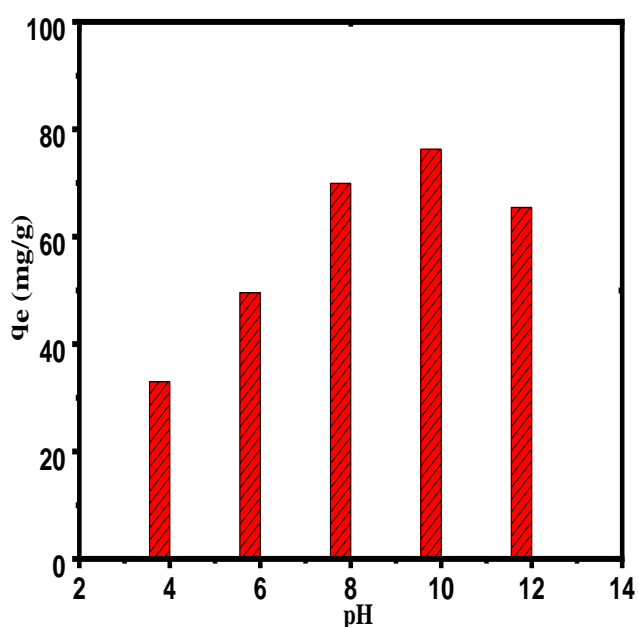
Fig 3: Effect of pH on the MB adsorption on UiO-66 MOF.

Fig 4: Effect of temperature on the adsorption of MB on UiO-66 MOF

3.3.2. Effect of temperature

The adsorption of MB occurred at various temperatures using 0.05 g MOF samples to estimate the thermodynamic parameters. Figure 4 depicts temperature's significance on the MB adsorption over UiO-66 MOF. The data demonstrate that MB adsorption decreases as temperature rises, which can be attributed to the weak attraction between MB and UiO-66 MOF due to the process's physisorption nature (34). The thermodynamic parameters were calculated using the equations below, [35] and the data are given in Table 1.

$$K_C = q_e/C_e$$

$$\ln(K_c) = \Delta S_{ads}/R - \Delta H_{ads}/RT$$

$$\Delta G_{ads} = \Delta H_{ads} - T\Delta S_{ads}$$

The fact that ΔH_{ads} is negative indicates that the MB adsorption process is exothermic. A decrease in the randomness state at the interface of the solid solution is indicated by a negative value of ΔS_{ads}. Negative ΔG_{ads} values indicate the adsorption process's spontaneity.

Table 1: Thermodynamic parameters for MB adsorption with UiO-66 MOF

MOF	K_c		ΔG^o_{ads} (kJ/mol)		ΔH^o_{ads}(kJ/mol)	ΔS^o_{ads}(J/mol K)
	298 K	318 K	298 K	318 K		
UIO-66	2.365	1.377	-5.3	-5.45	-5.7	-10. 33

3.3.3. Effect of the contact time

By altering the duration of balance between adsorbent and adsorbate, which is typically between 15 and 720 minutes, the rate of MB adsorption on MOFs was made possible. The adsorption capabilities of MB are depicted in Fig. 5 as a factor of contact time. The quantity adsorbed q_t is determined from the equation [36]:

$$q_t = (C_0 - C_t) V / .$$

The MB that was adsorbed at time t is denoted by the symbol qt. The initial MB concentrations are described by C_0, while the equilibrium MB concentrations are indicated with Ct. The MB solution's volume is V, and the adsorbent's mass is m. At initially, the MB adsorption on the UiO-66 MOF happens quickly, then slows over time until the equilibrium state is reached at 240 minutes, as shown in Fig 5.
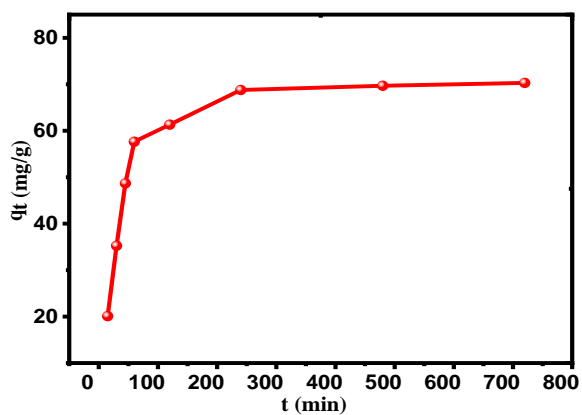
Fig 5: Effect of time on the adsorption of MB UiO-66 MOF.

3.3.4. Adsorption kinetics study

Through the analysis of pseudo 1st order and pseudo 2nd order models, the mechanism of the adsorption could be determined. The equation can be used to calculate the pseudo-1st order kinetic model's linear form [37]:

$$(q_e\text{-}q_t) = (q_e) - (k_1/2.303)$$

qe is the quantity of MB adsorbed at equilibrium while qt (mg/g) is the quantity of MB adsorbed at any given time (t). Then by graphing log(qe-qt) over time, one may get the pseudo first order model's rate constant, k1(min-1). Although the equation has the ability to find the pseudo-2nd order kinetic model's linear form [37]:

$$t/qt = 1/k_2qe^2 + t/qe$$

Where k_2 (g.mg^{-1}.min^{-1}) is the rate constant of pseudo-second order and the relationship between t/qt and time is displayed linearly. Table 2 lists the observed kinetic parameters and the correlation coefficient (R2).

The adsorption of UiO-66 MOF decided to follow the pseudo 2nd order kinetic model, however the pseudo 1st order model did not correspond to the experimental results, as shown in Figs. 6 and 7, as well as the data in Table 2. This is because there was a perfect fit between the estimated and observed values of adsorption capacity at equilibrium time (qe), and R2 values were greater than 0.99.

Sample name	Experimental q$_m$ (mg/g)	Pseudo 1st order kinetics			Pseudo 2nd order kinetics		
		q$_e$ (mg/g)	k$_1$(min^{-1})	R^2	q$_e$ (mg/g)	k$_2$(g.mg^{-1}.min^{-1})	R^2
UiO-66	70.29	40.317	1.44	0.963	73.26	0.0194	0.998

Table 2: Kinetic parameters for MB adsorption UiO-66 MOF.
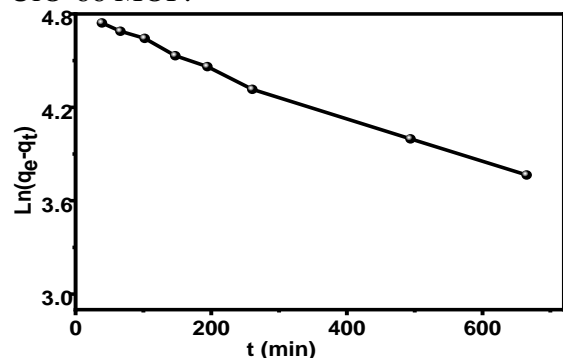
Fig 6: Pseudo 1st order kinetics for MB using UiO-66 MOF.
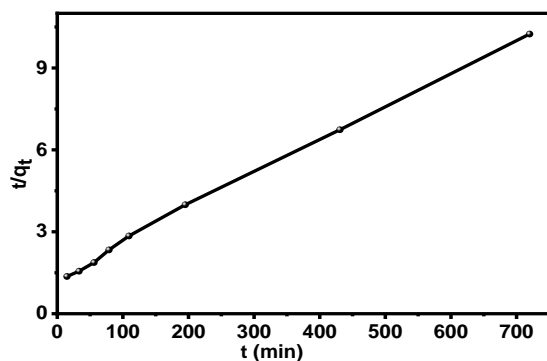
Fig 7: pseudo 2nd order kinetics for MB using UiO-66 MOF

3.3.5. Effect of the weight of UiO-66 MOF:

Fig 8 shows the influence of UiO-66 MOF weight on the removal of MB under fixed MB concentration and solution pH at 10 for MB was examined at 298 K. It was discovered that as catalyst weight is increased, MB adsorption decreases. This is can be attributed to the nature of the MOF surface [38] and covering or aggregation of UiO-66 adsorption sites, which reduces the UiO-66 MOF's surface area. [39, 40].
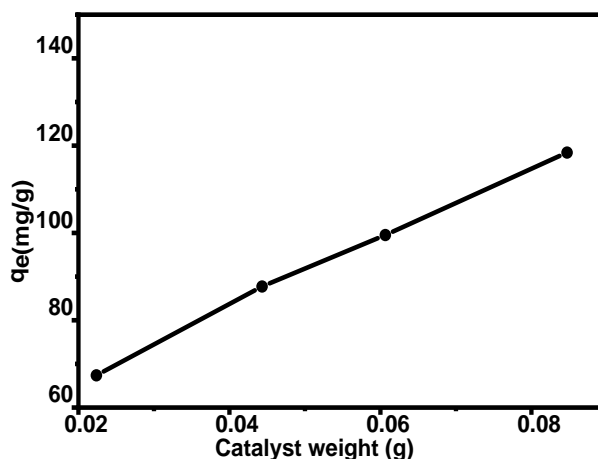
Fig 8: Effect of MOF weight on the adsorption of MB using UiO-66 MOF.

3.4.6. Effect of initial MB concentration

Figure 9 illustrates the impact of initial MB concentrations between 25 and 250 ppm on its removal percentage.
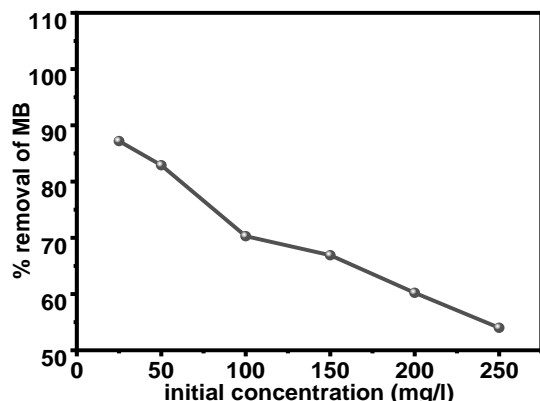
Fig 9: Effect of Initial concentration of MB on the adsorption using UiO-66 MOF.

3.3.7. Adsorption isotherms

Discovering the adsorption isotherms is crucial for understanding the adsorption system. Keeping the same weight of the adsorbent, MB adsorption on UiO-66 MOF was investigated at MB concentrations ranging from 25 to 250 ppm.

3.3.7.1. Langmuir isotherm

The equilibrium data for MB adsorption over UiO-66 MOF were fitted to Langmuir isotherms. The Langmuir isotherm model can be written as [41] :

$$q_e = \frac{K_L C_e}{1 + q_m C_e}$$

$$\frac{C_e}{q_e} = \frac{1}{K_L q_{max}} + \frac{C_e}{q_{max}}$$

When qe (mg/g) is the amount of adsorbed MB per gramme of Uio-66 and Ce (mg/L) is the MB equilibrium concentration. Langmuir's equilibrium constant is KL (L.g-1). The theoretical monolayer saturation capacity, qm, is denoted by KL/qm. A straight line with an intercept of 1/qmKL and a slope of 1/qm is shown on a plot of Ce/qe versus Ce. Due to the uniform distribution of active sites on the UiO-66 MOF surface, the experimental data was found to suit the Langmuir isotherm, as indicated by the coefficient of determination. Figure 10 depicts the linear plot characteristic of the Langmuir isotherm, which confirms the formation of a monolayer. One of the key properties of the Langmuir isotherm can be expressed using a separation factor, RL:

$$R_L = \frac{1}{1 + K_L C_o}$$

3.4.7.2. Freundlich isotherm

The adsorption of MB over UiO-66 MOF has also been studied using Freundlich isotherm. The Freundlich isotherm model can be written as [41]:

$$q_e = K_F C_e^{1/n}$$

$$\ln q_e = (1/n) \ln C_e + \ln K_F$$

Where 1/n is the adsorption intensity, n and KF are Freundlich constants deduced from the slope and intercept of the linear plot of ln qe versus ln Ce shown in Figure 11. Looking at Table 3, which provides the values of the Langmuir and Freundlich parameters, we discovered that the data of adsorption is better matched to the Langmuir model than the Freundlich model. The value of RL indicating the favorability of the process, and the value of R2.

Table 3: Langmuir and Freundlich parameters.

Sample name	Langmuir isotherm				Freundlich isotherm		
	q_m (mg/g)	K_L (L/mg)	R_L	R^2	K_F	1/n	R^2
UiO-66	165	0.03	05	0.97	127	1.95	098
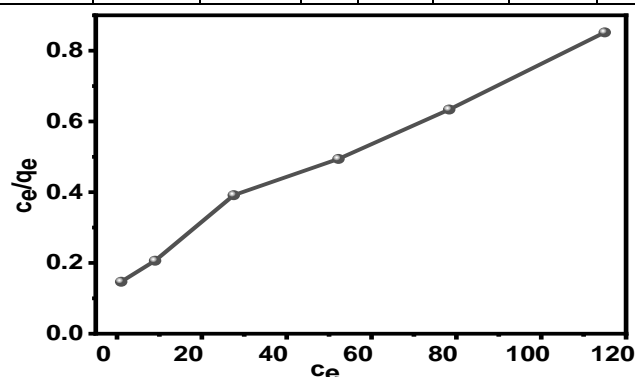
Fig 10: Langmuir Plot for MB using UiO-66 MOF.
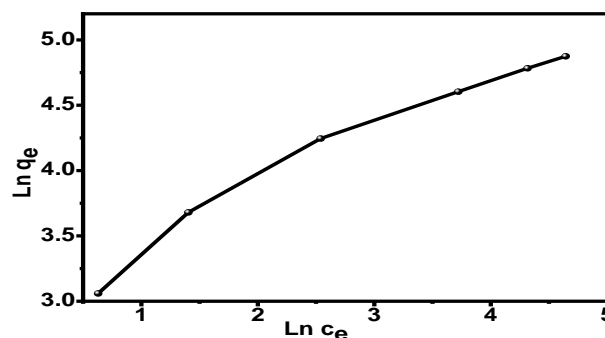
Fig 11: Freundlich Plot for MB using UiO-66 MOF.

4. Conclusions

In this work, methylene blue was removed from an aqueous solution by forming zirconium MOF (UiO-66) only by solvothermal techniques. The structure of UiO-66 was investigated via FTIR and SEM. The MB adsorption process, which denotes monolayer adsorption on UiO-66 MOF, was fitted by the Langmuir model. The pseudo-2nd order model is the kinetic model that most perfectly reflects the adsorption mechanism.

5. References

1. L. Wang, Y. Han, X. Feng, J. Zhou, P. Qi, B. Wang, (2016) Metal-organic frameworks for energy storage: Batteries and supercapacitors, Coord. Chem. Reviews **307** 361-381.

2. H. R. Abid, H. M. Ang, S. Wang, (2012) Effects of ammonium hydroxide on the structure and gas adsorption of nanosized Zr-MOFs (UiO-66), Nanoscale **4** 3089-3094.

3. J. Jiang, F. Gandara, Y. B. Zhang, K. Na, O. M. Yaghi, W. G. Klemperer, (2014) Superacidity in sulfated metal-organic framework-808, *J. Amer. Chem. Soc.* **136** 12844-12847.

4. Y.B. Zhang, H. Furukawa, N. Ko, W. Nie, H. J. Park, S. Okajima, K.E. Cordova, H. Deng, J. Kim, O.M. Yaghi, (2015) Introduction of functionality, selection of topology, and enhancement of gas adsorption in multivariate metal-organic framework-177, *J. Amer. Chem. Soc.* **137** 2641-2650.

5. Q. Zhou, Q. Gao, W. Luo, C. Yan, Z. Ji, P. Duan, (2015) One-step synthesis of amino-functionalized attapulgite clay nanoparticles adsorbent by hydrothermal carbonization of chitosan for removal of methylene blue from wastewater, Colloids and Surfaces A: Physicochem. Eng. Aspects **470** 248-257.

6. K. Manna, T. Zhang, M. Carboni, C. W. Abney, W. Lin, (2014) Salicylaldimine-based metal-organic framework enabling highly active olefin hydrogenation with iron and cobalt catalysts, *J. Amer. Chem. Soc.* **136** 13182–13185.

7. M. Carboni, C. W. Abney, S. Liu, W. Lin, (2013) Highly porous and stable metal-organic frameworks for uranium extraction, Chem. Sci. **4** 2396–2402.

8. M. Carboni, Z. Lin, C. W. Abney, T. Zhang, W. Lin, (2014) A metal-organic framework containing unusual eight-connected Zr-Oxo secondary building units and orthogonal carboxylic acids for ultra-sensitive metal detection, *Chem. Eur. J.* **20** 14965–14970.

9. F. Gandara, H. Furukawa, S. Lee, O.M. Yaghi, (2014) High methane storage capacity in aluminum metal-organic frameworks, *J. Amer. Chem. Soc.* **136** 5271-5274.

10. S. Lin, Z. Song, G. Che, A. Ren, P. Li, C. Liu, J. Zhang, (2014) Adsorption behavior of metal-organic frameworks for methylene blue from aqueous solution, Micropor. Mesopor. Mater. 193 27-34.

11. I. Ahmed, S. H. Jhung, (2014) Composites of metal-organic frameworks: Preparation and application in adsorption, Mater. Tod. **17** 136-146.

12. H. Furukawa, K. E. Cordova, M. O'Keeffe, O. M. Yaghi, (2013) The Chemistry and Applications of Metal-Organic Frameworks, Science **341** 1230444.

13. J. H. Cavka, S. Jakobsen, U. Olsbye, N. Guillou, C. Lamberti, S. Bordiga, K.P. Lillerud, (2008) A New Zirconium Inorganic Building Brick Forming Metal-Organic Frameworks with Exceptional Stability, *J. Amer. Chem. Soc.* **130** 13850–13851.

14. F. Vermoortele, B. Bueken, G. Le Bars, B. Van de Voorde, M. Vandichel, K. Houthoofd, A. Vimont, M. Daturi, M. Waroquier, V. Van Speybroeck, C. Kirschhock, D. E. De Vos, (2013) Synthesis Modulation as a Tool To Increase the Catalytic Activity of Metal–Organic Frameworks: The Unique Case of UiO-66(Zr), *J. Amer. Chem. Soc.* **135** 11465–11468.

15. J. Kim, S.-N. Kim, H.-G. Jang, G. Seo, W.-S. Ahn, (2013) CO_2 cycloaddition of styrene oxide over MOF catalysts, Appl. Catal. A Gen. **453** 175–180.

16. M. Saito, T. Toyao, K. Ueda, T. Kamegawa, Y. Horiuchi, M. Matsuoka, (2013) Effect of pore sizes on catalytic

activities of arenetricarbonyl metal complexes constructed within Zr-based MOFs, Dalton Trans. **42** 9444– 9447.

17. Y. Shao, X. Wang, Y. Kang, Y. Shu, Q. Sun, L. Li, (2014) Application of Mn/MCM-41 as an adsorbent to remove methyl blue from aqueous solution, *Journal of Colloid and Interface Science* **429** 25-33.

18. C. Belpaire, T. Reyns, C. Geeraerts, J. Van Loco, (2015) Toxic textile dyes accumulate in wild European eel Anguilla anguilla, Chemosphere 138 784-791.

19. H. Hayat, Q. Mahmood, A. Pervez, Z.A. Bhatti, S.A. Baig, (2015) Comparative decolorization of dyes in textile wastewater using biological and chemical treatment, Sep. Purif. Techn. **154** 149-153.

20. F. Tan, M. Liu, K. Li, Y. Wang, J. Wang, X. Guo, G. Zhang, C. Song, (2015) Facile synthesis of size-controlled MIL-100(Fe) with excellent adsorption capacity for methylene blue*, Chem. Eng. J.* **281** 360-367.]

21. T. Shen, J. Luo, S. Zhang, X. Luo, (2015) Hierarchically mesostructured MIL-101 metal-organic frameworks with different mineralizing agents for adsorptive removal of methyl orange and methylene blue from aqueous solution, *J. Environ. Chem. Eng.* **3** 1372-1383.

22. Z. Wu, H. Zhong, X. Yuan, H. Wang, L. Wang, X. Chen, G. Zeng, Y. Wu, (2014) Adsorptive removal of methylene blue by rhamnolipid-functionalized graphene oxide from wastewater, Water Research **67** 330-344.

23. A. Asfaram, M. Ghaedi, S. Hajati, A. Goudarzi, E.A. Dil, (2017) Screening and optimization of highly effective ultrasound-assisted simultaneous adsorption of cationic dyes onto Mn-doped Fe_3O_4-nanoparticle-loaded activated carbon, Ultr. Sonochem. 34 1-12.

24. E. A. Dil, M. Ghaedi, A. Ghaedi, A. Asfaram, M. Jamshidi, M.K. Purkait, (2016)Application of artificial neural network and response surface methodology for the removal of crystal violet by zinc oxide nanorods loaded on activated carbon: kinetics and equilibrium

25. E. Haque, J. E. Lee, I. T. Jang, Y. K. Hwang, J. S. Chang, J. Jegal, S. H. Jhung, (2010) Adsorptive removal of methyl orange from aqueous solution with metal-organic frameworks, porous chromium-benzenedicarboxylates, *J. Hazard. Mater.***181** 535-542.

26. E. R. Garcıa, R. L. Medina, M. M. Lozano, I. H. Perez, M. J. Valero, A. M. M. Franco, (2014) Adsorption of azo-dye orange II from aqueous solutions using a metal-organic framework material: Iron-Benzenetricarboxylate, Materials **7** 8037–8057.

27. X. Zhao, S. Liu, Z. Tang, H. Niu, Y. Cai, W. Meng, F. Wu, J. P. Giesy, (2015) Synthesis of magnetic metal-organic framework (MOF) for efficient removal of organic dyes from water. Sci Rep **5** 1–10.

28. H. Guo, F. Lin, J. Chen, F. Li, W. Weng, (2015) Metal-organic framework MIL-125(Ti) for efficient adsorptive removal of Rhodamine B from aqueous solution. Appl. Organomet. Chem. **29** 12–19.

29. A. Abbasi, M. Soleiman, M. Najafi, S. Geranmayeh, (2016) New interpenetrated mixed (Co/Ni) metal-organic framework for dye removal under mild conditions. Inorg. Chim. Acta. 439 18–23.

30. J. H. Cavka, S. Jakobsen, U. Olsbye, N. Guillou, C. Lamberti, S. Bordiga, K. P. Lillerud, (2008) A new zirconium inorganic building brick forming metal-organic frameworks with exceptional stability, *Journal of the American Chemical Society* **130** 13850-13851.

31. L. Valenzano, B. Civalleri, S. Chavan, S. Bordiga, M.H. Nilsen, S. Jakobsen, K.P. Lillerud, C. Lamberti, (2011) Disclosing the complex structure of UiO-66 metal organic framework: A synergic combination of experiment and theory, Chemistry of Materials **23** 1700-1718.

32. Z. Zhang, Z. Z. Yao, S. Xiang, B. Chen, (2014) Perspective of microporous metal–organic frameworks for CO_2 capture and separation, Energy Environ. Sci. 7 2868–2899.

33. W. S. Abo El-Yazeed, Y. G. Abou El-Reash, L. A. Elatwy, Awad I. Ahmed,

(2020) Facile fabrication of bimetallic Fe–Mg MOF for the synthesis of xanthenes and removal of heavy metal ions, RSC Adv. **10** 9693-9703.

34. W. S. Abo El-Yazeed, Y. G. Abou El-Reash, L. A. Elatwy, Awad I. Ahmed, (2020) Novel bimetallic Ag-Fe MOF for exceptional Cd and Cu removal and 3,4-dihydropyrimidinone synthesis, *J. Taiwan Instit. Chem. Eng.* **114** 199-210.

35. H. Wang, X. z. Yuan, Y. Wu, H. Huang, G. Zeng, Y. Liu, X. Wang, N. Lin, Y. Qi., (2013) Adsorption characteristics and behaviors of graphene oxide for Zn(II) removal from aqueous solution, *J. Appl. Surf. Sci.* **279** 432-440.

36. J. Zhang, Z. Xiong, L .Chen, W. Chunsheng, (2016) Exploring a thiol-functionalized MOF for elimination of lead and cadmium from aqueous solution, *J.Mol.Liquids* **221** 43-50.

37. S. Chowdhury, R. Mishra, P. Saha, (2011) Adsorption thermodynamics, kinetics and isosteric heat of adsorption of malachite green onto chemically modified rice husk, Desalination, **265** 159 –168.

38. A. Asfaram, M. Ghaedi, S. Hajati, M. Rezaeinejad, A. Goudarzi, Purkait M. K., (2015) Rapid removal of Auramine-O and Methylene blue by ZnS: Cu nanoparticles loaded on activated carbon: A response surface methodology approach, *J. Taiwan Inst. Chem. Eng.* **53** 80 –91.

39. S. Chala, K. Wetchakun, S. Phanichphant, B. Inceesungvorn, (2014) Enhanced visible-light-response photocatalytic degradation of methylene blue on Fe-loaded $BiVO_4$ photocatalyst, *J. Alloys and Compounds*, **597** 129-135.

40. A. Maleki, B. Hayati, M. Naghizadeh, S. W. Joo, (2015)Adsorption of hexavalent chromium by metal-organic frameworks from aqueous solution. *J Ind. Eng. Chem.* **28** 211–216.

41. N. Zhang , X. Yang, X. Yu, Y. Jia , J. Wang, L. Kong, Z. Jin, B. Sun, T. Luo, J. Liu, (2014) Al-1,3,5-benzene tricarboxylic metal-organic frameworks: a promising adsorbent for defluoridation of water with pH insensitivity and low aluminum residual. *Chem. Eng. J.* **252** 220–229.

42. S. A. El-Hakam, A. A. Ibrahim, L. A. Elatwy, W. S. Abo El-Yazeed, R. S. Salama, Y. G. Abou El-Reash, A. I. Ahmed, (2021) Greener route for the removal of toxic heavy metals and synthesis of 14-aryl-14H dibenzo[a,j] xanthene using a novel and efficient Ag-Mg bimetallic MOF as a recyclable heterogeneous nanocatalyst, *J. Taiwan Inst. Chem. Eng*. **122** 176-189.